

## The Structure of Isolated Thalidomide as Reference for its Chirality-Dependent Biological Activity: A Laser-Ablation Rotational Study.

Susana Blanco,<sup>\*a</sup> Alberto Macario,<sup>a</sup> and Juan Carlos López<sup>\*a</sup>

<sup>a</sup> Prof. S. Blanco, Dr. A. Macario, Prof. J. C. López,  
Departamento de Química Física y Química Inorgánica, Facultad de Ciencias, IU CINQUIMA, Universidad de Valladolid, 47011  
Valladolid, Spain.  
E-mail: [susana.blanco@uva.es](mailto:susana.blanco@uva.es), [alberto.macario@uva.es](mailto:alberto.macario@uva.es), [juancarlos.lopeza@uva.es](mailto:juancarlos.lopeza@uva.es)

### Corresponding Author

\* E mail: [juancarlos.lopeza@uva.es](mailto:juancarlos.lopeza@uva.es); [susana.blanco@uva.es](mailto:susana.blanco@uva.es)

### ELECTRONIC SUPPORTING INFORMATION

#### Table of contents:

- **Complete reference 37**
- **Comparison of the results obtained on *o*-anisic acid for heating and laser ablation vaporization methods**
- **Figure S1.** Observed species in the spectra of *o*-anisic acid.
- **Figure S2.** Comparison between the *o*-anisic acid CP-FTMW spectra in the 6-8 GHz frequency region obtained employing the laser ablation nozzle and the heating nozzle.
- **Figure S3.** a) Ring-bending and ring-twisting coordinates for puckering of glutarimide.  
b) DFT Potential energy function (B3LYP-D3BJ/cc-pVDZ) for the interconversion of the two bent equivalent configurations of glutarimide.
- **Figure S4.** DFT Potential energy function (B3LYP-D3BJ/cc-pVDZ) for the interconversion of TD-eq and TD-ax configurations of thalidomide.
- **Figure S5.** Comparison of the potential energy profile along the ring-bending coordinate (see Figures S3 and S4) of glutarimide (blue) and thalidomide (orange).
- **Figure S6.** DFT Potential energy function (B3LYP-D3BJ/cc-pVDZ) for the pure ring-bending of thalidomide
- **Figure S7.** Comparison of the potential energy profile for ring-puckering of thalidomide.
- **Figure S8.** DFT Potential energy function (B3LYP-D3BJ/cc-pVDZ) of thalidomide for the pure glutarimide ring twisting coordinate.

- **Figure S9.** DFT Potential energy profile (B3LYP-D3BJ/cc-pVDZ) of thalidomide for internal rotation of phthalimide.

- **Table S1.** Relative intensities for the *o*-anisic acid monomer conformations with respect to the most intense species observed (T1) of the most intense spectra (Ar LA).

- **Table S2.** Comparison of the intensities for the *o*-anisic acid monomer and water complex conformations, salicylic acid (Sal A.), methyl salicylate (Sal M.), and Methyl 2-methoxybenzoate (M2M) observed species relative to the most intense species (T1) of each spectrum.

- **Table S3.** Predicted coordinates of the molecular structure of TD-eq conformer calculated at B3LYP-D3BJ/cc-pVDZ level of theory.

- **Table S4.** Predicted coordinates of the molecular structure of TD-eq conformer calculated at MP2/6-311++G(2d,p) level of theory.

- **Table S5.** Predicted coordinates of the molecular structure of TD-ax conformer calculated at B3LYP-D3BJ/cc-pVDZ level of theory.

- **Table S6.** Predicted coordinates of the molecular structure of TD-ax conformer calculated at MP2/6-311++G(2d,p) level of theory.

- **Table S7.** Observed rotational transitions and residuals (all the values in MHz) for the TD-eq conformer of thalidomide in the ground vibrational state.

### **Complete reference 37**

Gaussian16, rev. A.03, Frisch, M. J.; Trucks, G. W.; Schlegel, H. B.; Scuseria, G. E.; Robb, M. A.; Cheeseman, J. R.; Scalmani, G.; Barone, V.; Petersson, G. A.; Nakatsuji, H.; Li, X.; Caricato, M.; Marenich, A. V.; Bloino, J.; Janesko, B. G.; Gomperts, R.; Mennucci, B.; Hratchian, H. P.; Ortiz, J. V.; Izmaylov, A. F.; Sonnenberg, J. L.; Williams-Young, D.; Ding, F.; Lipparini, F.; Egidi, F.; Goings, J.; Peng, B.; Petrone, A.; Henderson, T.; Ranasinghe, D.; Zakrzewski, V. G.; Gao, J.; Rega, N.; Zheng, G.; Liang, W.; Hada, M.; Ehara, M.; Toyota, K.; Fukuda, R.; Hasegawa, J.; Ishida, M.; Nakajima, T.; Honda, Y.; Kitao, O.; Nakai, H.; Vreven, T.; Throssell, K.; Montgomery Jr., J. A.; Peralta, J. E.; Ogliaro, F.; Bearpark, M. J.; Heyd, J. J.; Brothers, E. N.; Kudin, K. N.; Staroverov, V. N.; Keith, T. A.; Kobayashi, R.; Normand, J.; Raghavachari, K.; Rendell, A. P.; Burant, J. C.; Iyengar, S. S.; Tomasi, J.; Cossi, M.; Millam, J. M.; Klene, M.; Adamo, C.; Cammi, R.; Ochterski, J. W.; Martin, R. L.; Morokuma, K.; Farkas, O.; Foresman, J. B.; Fox, D. J. Gaussian, Inc., Wallingford CT, 2016.

## **Comparison of the results obtained on *o*-anisic acid for heating and laser ablation vaporization methods**

To test the new laser ablation system we have used *o*-anisic acid (m.p. of 106 °C) previously studied<sup>1</sup> using the same CP-FTMW spectrometer and a heatable nozzle held at a temperature of 150 °C. Its rotational spectrum is rich in a wide range of species including three monomer conformers, T1, C1, C2, two conformers of the monohydrated complex, T1-w-1, C2-w-1, and three identified decomposition products, salicylic acid, methyl salicylate, and methyl-2-methoxy benzoate (See Figure S1). The comparison of these results with those of laser ablation vaporization would give us important information about the performance of the new laser ablation nozzle. We collected height different spectra of *o*-anisic acid in the 6-8 GHz frequency region employing both heating and laser ablation nozzles, using Ar or Ne as carrier gases, and inserting or not a water reservoir in the carrier gas line before the nozzle, which can be necessary to form microsolvated complexes.

All the spectra were taken with the same number of averages (800 kAv), to obtain the same S/N ratio. This number of averages was enough to observe all the desired species. In all cases, the stagnation pressures, the molecular pulse width, and the laser trigger delays were optimized to obtain the highest possible spectral intensities. The backing pressure employed with Ar was 6 bar for laser ablation and 3 bar for heating with molecular pulses of 900 µs. Employing Ne pressures between 2-3 bar were used in both cases with a molecular pulse width of 700 µs. In all experiments, laser shot delays of over 700 µs were used. In the four dense rotational spectra recorded with the laser ablation method, all rotational lines disappeared when the laser beam was turned off.

The first interesting fact is that laser ablation vaporization leads to observed rotational lines with higher J values indicating higher rotational temperatures. Moreover, to compare the spectra among them we have employed relative intensity measurements. The most intense spectra were obtained using laser ablation with Ar while using heating methods the most intense spectra were observed with Ne. These spectra are compared in Figure S2. The most intense spectrum corresponds to conformer T1 of *o*-anisic acid so it has been taken as a reference. Table S1 gives a comparison of the relative intensities of the spectra of the monomer species observed referred to the spectrum of T1 recorded with Ar in absence of water and by laser ablation. This intensity is almost double as the most intense spectrum recorded using heating methods and Ne in absence of water as the carrier gas.

When we compare the results obtained for T1 with Ar and both vaporization methods one can see that the intensity of the spectrum recorded using laser ablation is more than three times higher than that obtained by heating. In contrast, in the case of Ne, the intensities of the spectrum recorded by both vaporization methods are almost equal. The addition of water vapor to the carrier gas in all cases reduces the intensity to about half of the value obtained without the water addition.

We have also compared the intensity of all species observed relative to the most intense species (T1) independently for each experiment (Table S2). The intensities for different molecules or adducts were done by comparing the most intense lines in each case. The observations for the *o*-anisic acid monomer can be associated to an increase of the vibrational temperature in the expansion when the laser ablation system is employed. The changes between the different methods are critical in the case of the less stable monomer species with intensities that neatly increase when using laser ablation. Laser ablation increases the relative intensity of the *o*-anisic low stability conformers (C1 and C2) in all the cases with respect to those observed using the heating nozzle. This is also applicable to the case of the first vibrationally excited state of C2 conformer (C2(0<sup>-</sup>)), which has been detected in the spectra using laser ablation but is close to the limit of the detection in the heating spectra.

Monohydrated complexes of *o*-anisic acid are an interesting benchmark for laser ablation. It is important to note that these monohydrates are present in the expansion even if no water reservoir is added to the gas line, indicating the presence of small amounts of water in the carrier gas, in the gas line or in the sample as the water of crystallization. The most intense species observed is the monohydrate of T1 monomer form labeled T1-w-1. As can be seen in Figure 2 the spectra for this species is rather intense, being the most intense lines of this complex about ¾ of the intensity of the most intense lines of monomer T1 form. Table S1 also collects the relative intensity measurements of the monohydrated complexes relative to the most intense spectrum observed when heating with Ne. The use of laser ablation reduces the intensity of T1-w-1 lines to 10-20% of the observed intensities with heating methods. In the case of the weaker complex, C2-w-1, it simply disappears from the spectrum. Although the intensities of the hydrated species are considerably lower in laser ablation spectra, it is worth remarking that using our laser ablation system complexes can be detected in favorable conditions.

The differences observed in the behavior of the carrier gases deserve some discussion. Ar is more efficient than Ne to get more intense monomer spectra employing the laser

ablation method. This happens for a wide range of stagnation pressure. In contrast, in the spectra obtained with the laser ablation nozzle, the most energetic conformers ( $C1$ ,  $C2(0^+)$  and  $C2(0^-)$ ) have higher intensity ratios when Ne is employed instead of Ar as a carrier gas, being this more pronounced for the  $C2(0^-)$  excited state. The results in Tables S1 and S2 also reveal that Ne is more efficient in the formation of water complexes with both vaporization methods. The presence of water vapor in the gas flow alters to some extent the observed behavior probably due in part to the formation of complexes.

In our previous paper on *o*-anisic acid<sup>1</sup>, the spectra of salicylic acid, methyl salicylate, and methyl-2-methoxy benzoate and their water complexes were also observed. These were identified by mass spectrometry as decomposition products. The formation of these compounds from *o*-anisic acid can be idealized from isodesmic reactions that exchange the methyl group among the different molecules. Interestingly the spectra of these species, which enhance when adding water vapor to the gas line, disappear when using laser ablation. This confirms that these are products of thermal decomposition of *o*-anisic acid and justify why laser ablation is an efficient method of vaporization in cases of thermally labile samples.

The main differences observed in the spectra recorded using both methods could be attributed to changes in the temperatures of the jet caused by two complementary facts. Laser ablation is a complex process that may result in high translational temperatures and collisionally induced vibration and rotational cooling in the laser plume.<sup>2</sup> However, the laser plume crosses with the expanding Ar or Ne flow in the seeding region near the throat of the nozzle where laser-ablated molecules are dragged into the expansion by colliding with the carrier gas atoms. The fact that the Ar collision section is greater than that of Ne can be the cause of being efficient in dragging the ablated molecules into the jet expansion. The seeding region is where the collisional cooling starts so the design of the laser ablation nozzle could affect the shape of the expansion, causing a higher spread of the velocity distribution and increasing the translational temperature. Also, the post-desorption collisions which occur in the seeding region immediately after the laser ablation might affect population distributions in the expansion, altering the rotational and vibrational temperatures.<sup>2</sup> The seeding region where the laser plume and the expanding gas cross is close to the throat of the nozzle, is where ternary collisions are still high enough to form clusters. The laser ablation plume probably disrupts clustering formation resulting in a lower cluster concentration.

- 1 J. C. López, A. Macario and S. Blanco, *Phys. Chem. Chem. Phys.*, 2019, **21**, 6844–6850.
- 2 R. J. Levis, *Annu. Rev. Phys. Chem.*, 1994, **45**, 483–518.

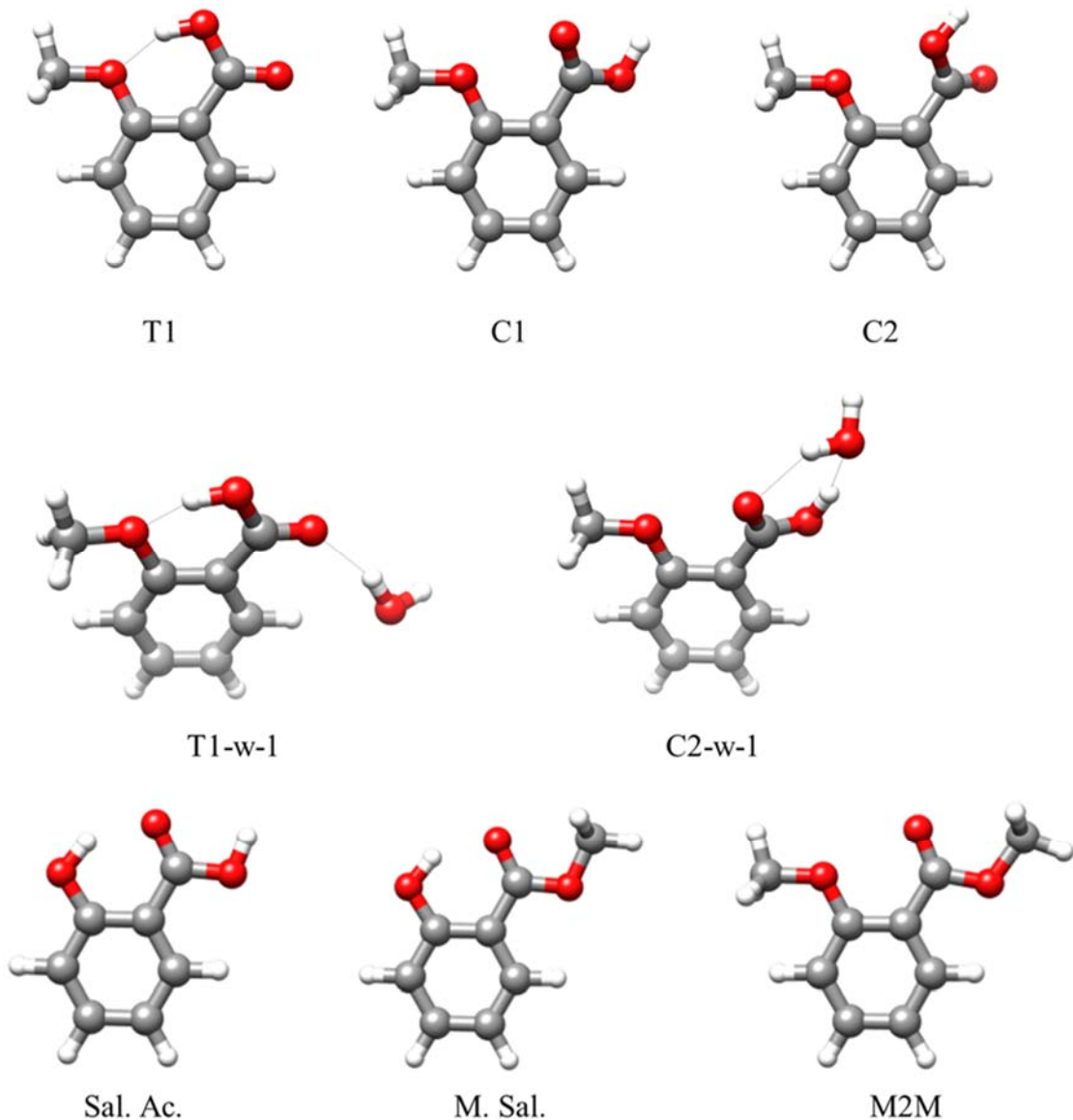


**Figure S1.** Observed species in the spectra of *o*-anisic acid including the *o*-anisic acid monomer conformers (T1, C1 and C2), their monohydrated cluster conformations (T1-w-1 and C2-w-1) and their decomposition products salicylic acid (Sal. Ac.), methyl salicylate (M. Sal.) and methyl 2-methoxybenzoate (M2M).

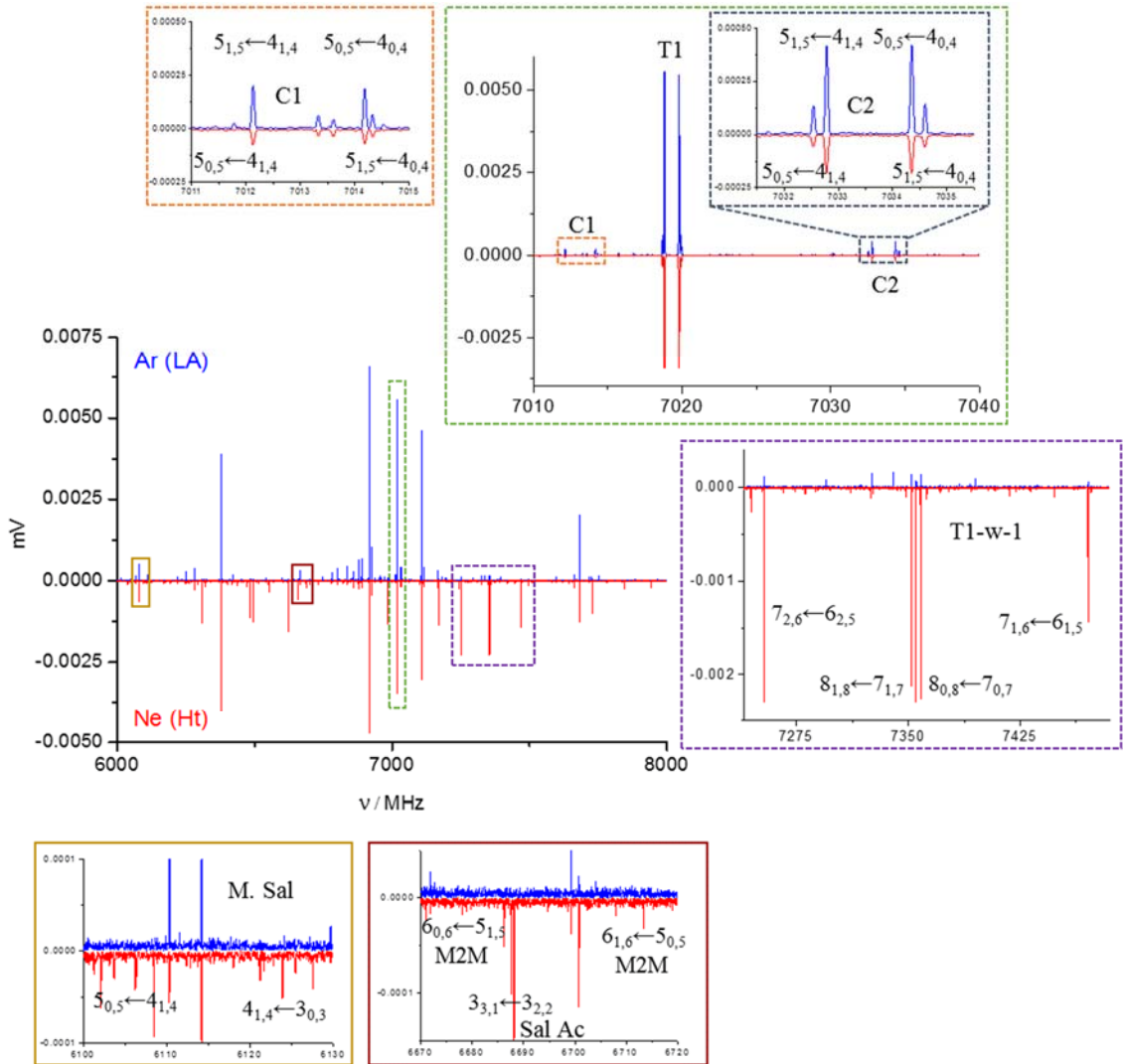


**Figure S2.** Comparison between the *o*-anisic acid CP-FTMW spectra in the 6-8 GHz frequency region employing the laser ablation nozzle (LA) with Ar as carrier gas (blue spectrum) and the heating nozzle (Ht) with Ne as carrier gas (red spectrum). Both spectra were taken with the same number of averages (800kAv), obtaining a similar S/N ratio. The green excerpt shows the *o*-anisic acid monomer conformers, with a higher intensity in the LA than in the Ht spectra. The orange and blue zooms show a typical  $\mu_a$ - and  $\mu_b$ -type pattern quadruplet of the transitions  $5_{0,5} \leftarrow 4_{1,4}$ ;  $5_{1,5} \leftarrow 4_{1,4}$ ;  $5_{0,5} \leftarrow 4_{0,4}$  and  $5_{1,5} \leftarrow 4_{0,4}$  by the C1 and C2 *o*-anisic acid monomer conformations. The purple excerpt shows the transitions  $7_{2,6} \leftarrow 6_{2,5}$ ;  $5_{1,8} \leftarrow 7_{1,7}$ ;  $8_{0,8} \leftarrow 7_{0,7}$  and  $7_{1,6} \leftarrow 6_{1,5}$  of the most intense T1-w-1 conformer of the *o*-anisic acid water complex. The yellow and brown excerpts show the decomposition products of *o*-anisic acid. The yellow excerpt shows the transitions  $5_{0,5} \leftarrow 4_{1,4}$  and  $4_{1,4} \leftarrow 3_{0,3}$  of the methyl salicylate (M. Sal.), while the brown excerpt shows the transition  $3_{3,1} \leftarrow 3_{2,2}$  of salicylic acid (Sal. Ac.) and the transitions  $6_{0,6} \leftarrow 5_{1,5}$  and  $6_{1,6} \leftarrow 5_{0,5}$  of methyl-2-methoxybenzoate (M2M).

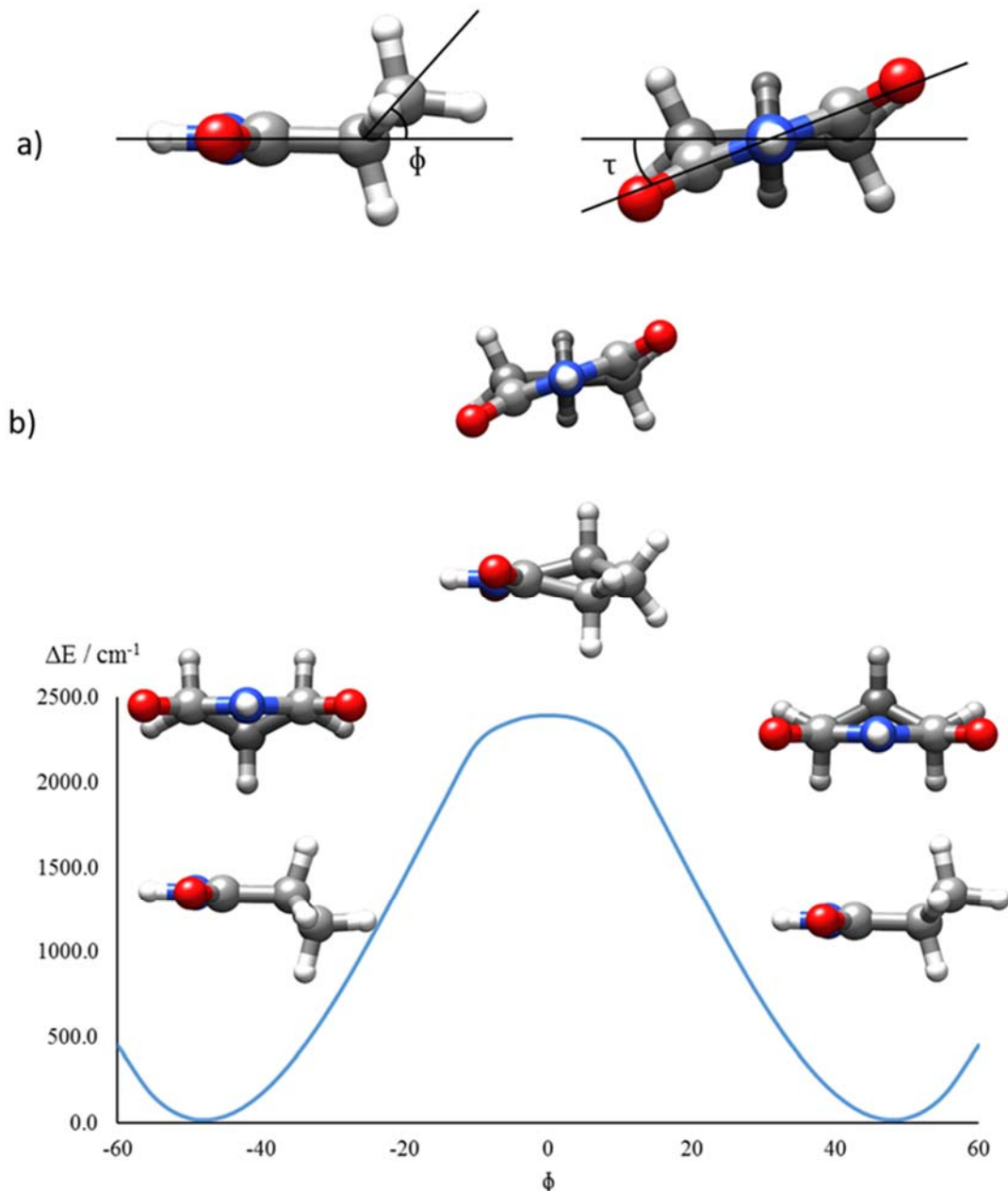


**Figure S3.** a) Ring-bending and ring-twisting coordinates for puckering of glutarimide: b) DFT Potential energy function (B3LYP-D3BJ/cc-pVDZ) for the interconversion of the two bent equivalent configurations of glutarimide. The equilibrium configuration is a purely bent configuration with  $C_s$  symmetry. All ring atoms, N<sub>1</sub>, C<sub>2</sub>, C<sub>3</sub>, C<sub>5</sub> and C<sub>6</sub>, are in a plane except the C<sub>4</sub> atom which is predicted to be out of plane with a bending angle  $\phi = \pm 48^\circ$ . The configuration for  $\phi = 0^\circ$  has not a planar ring but it corresponds to a  $C_2$  symmetry with twisting angle of  $\tau = \pm 16.4^\circ$ .

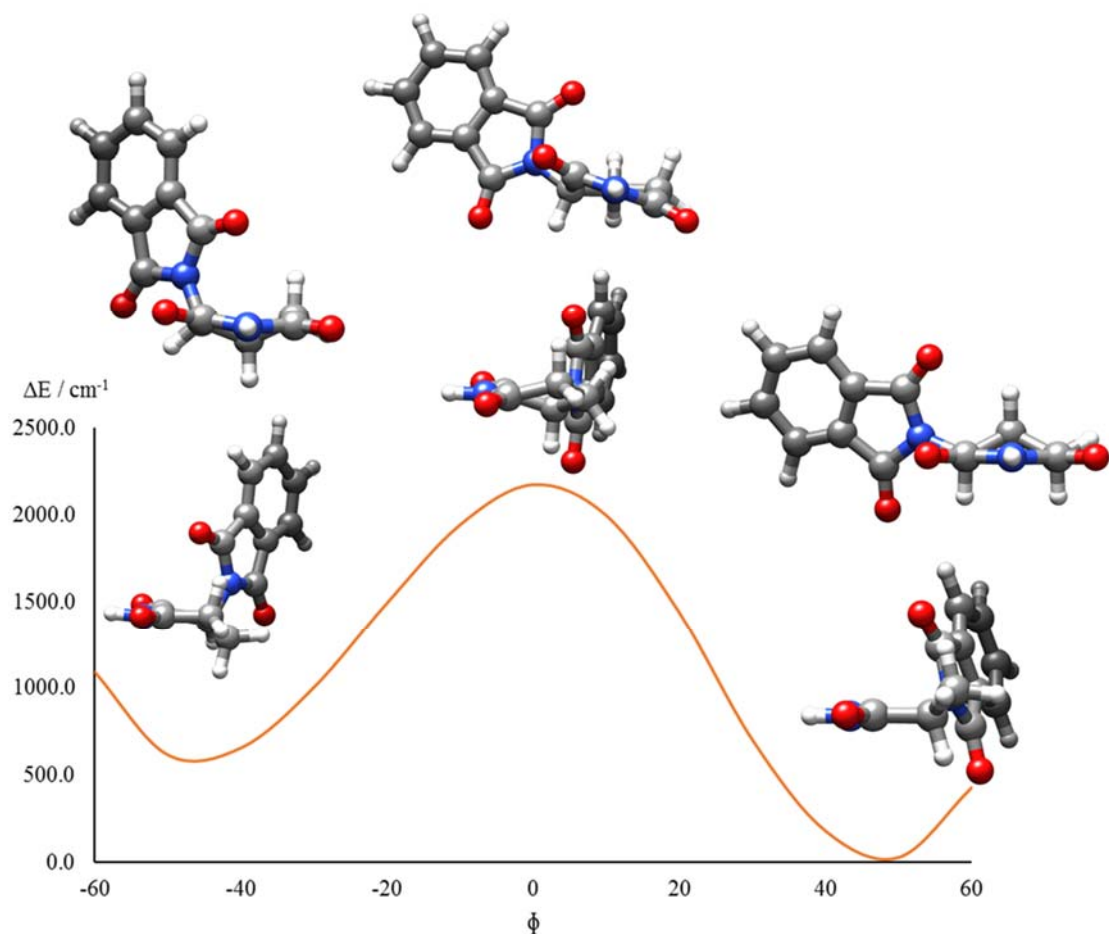


**Figure S4.** DFT Potential energy function (B3LYP-D3BJ/cc-pVDZ) for the interconversion of TD-eq and TD-ax configurations of thalidomide. The interconversion coordinate is the  $\phi$  angle for the bending of carbon C4 of the glutarimide moiety (see Figure S3). The TD-eq global minimum corresponds as in glutarimide as a purely bent configuration of this moiety with ring atoms, N1, C2, C3, C5, and C6, in a plane except for the C4 atom which is predicted to be out of the plane with a bending angle  $\phi = 48.3^\circ$ . As in glutarimide, the configuration for  $\phi = 0^\circ$  corresponds is a twisted configuration with  $\tau = -17.9^\circ$ . For the TD-ax form the glutarimide ring is a mixed configuration with  $\phi = 46.1^\circ$  and  $\tau = -6^\circ$ . Comparing this data with those of glutarimide it can be deduced that TD-eq has essentially a non-distorted glutarimide ring while in TD-ax a distorted glutarimide ring is predicted probably due to steric interactions.

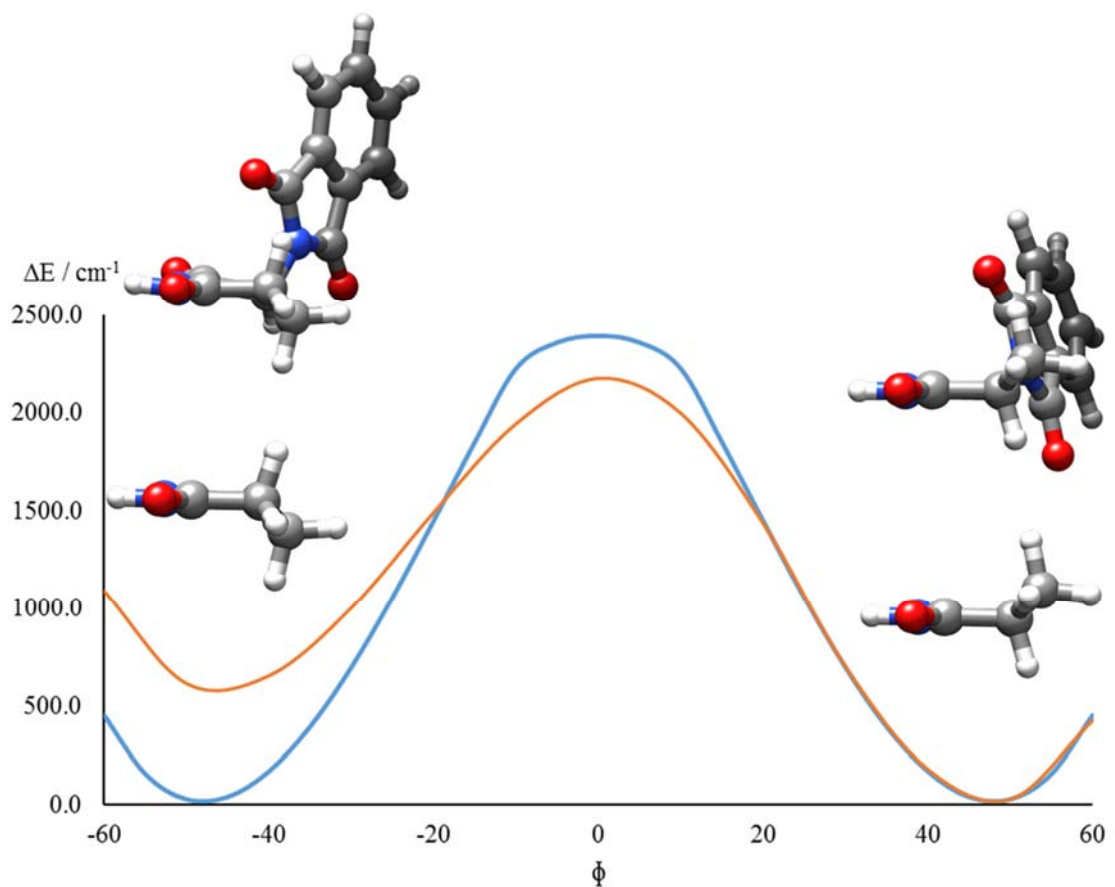


**Figure S5.** Comparison of the potential energy profile along the ring-bending coordinate (see Figures S3 and S4) of glutarimide (blue) and thalidomide (orange). Both potential energy functions are almost equal around the equatorial form well of thalidomide. The distortion induced in the glutarimide ring by phthalimide in the axial form leads to higher energy for this form.

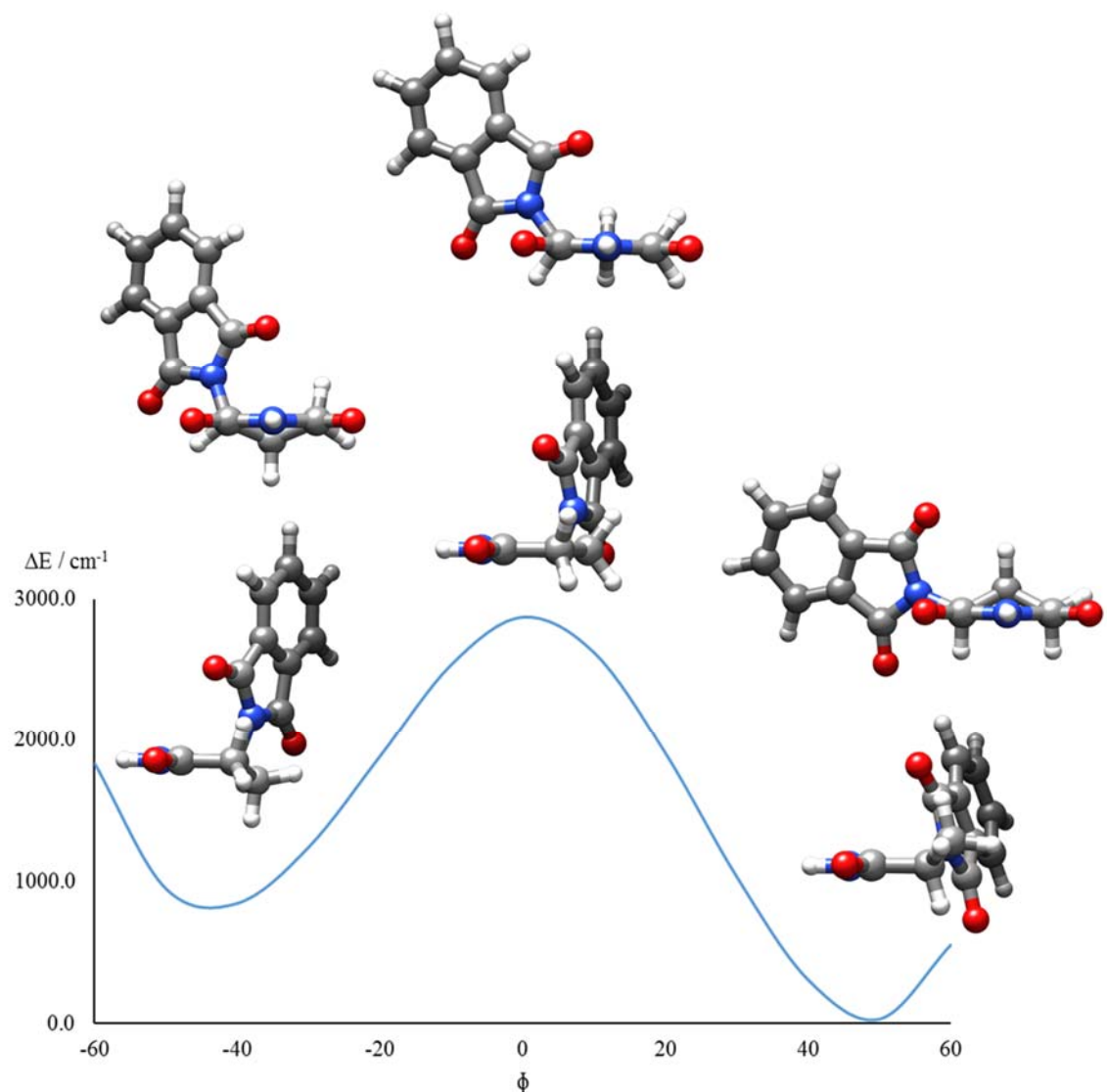


**Figure S6.** DFT Potential energy function (B3LYP-D3BJ/cc-pVDZ) for the pure ring-bending of thalidomide along the ring-bending coordinate (see Figure S3), fixing the all ring atoms, N<sub>1</sub>, C<sub>2</sub>, C<sub>3</sub>, C<sub>5</sub> and C<sub>6</sub>, to the plane with the exception of C<sub>4</sub> atom, so the twisting angle  $\tau$  was forced to be 0° in all the steps.

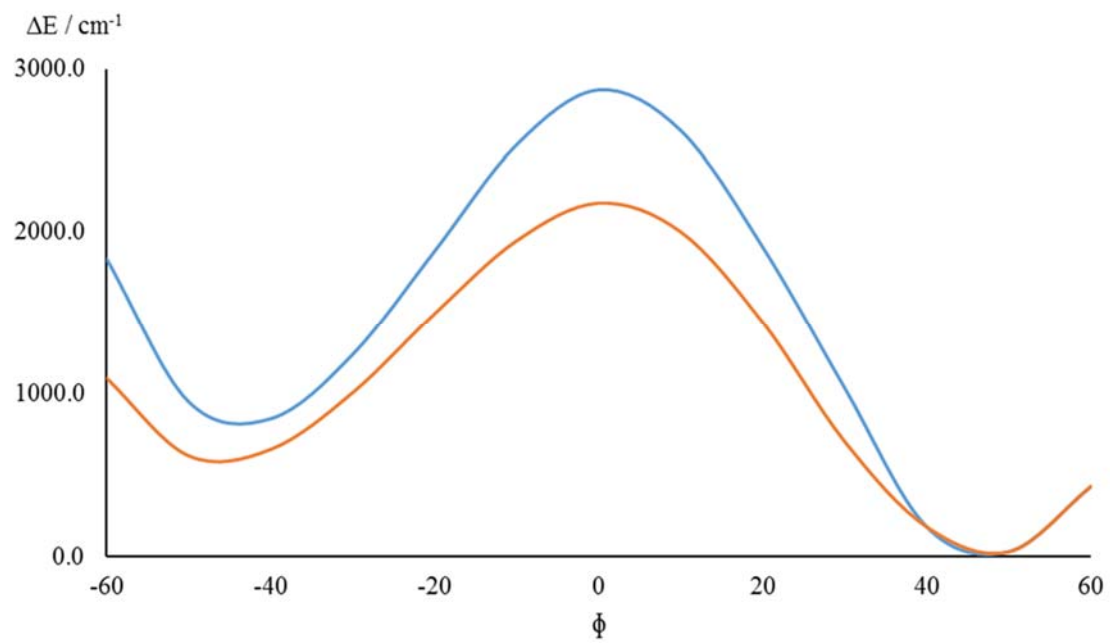


**Figure S7.** Comparison of the potential energy profile for ring-puckering of thalidomide. In blue is shown the profile for the pure ring-bending shown in Figure S6 and in orange the potential energy function shown in Figure S4 for a relaxed scan in which ring-twisting is allowed to occur, both of them defined through the ring-bending coordinate (see Figure S3).

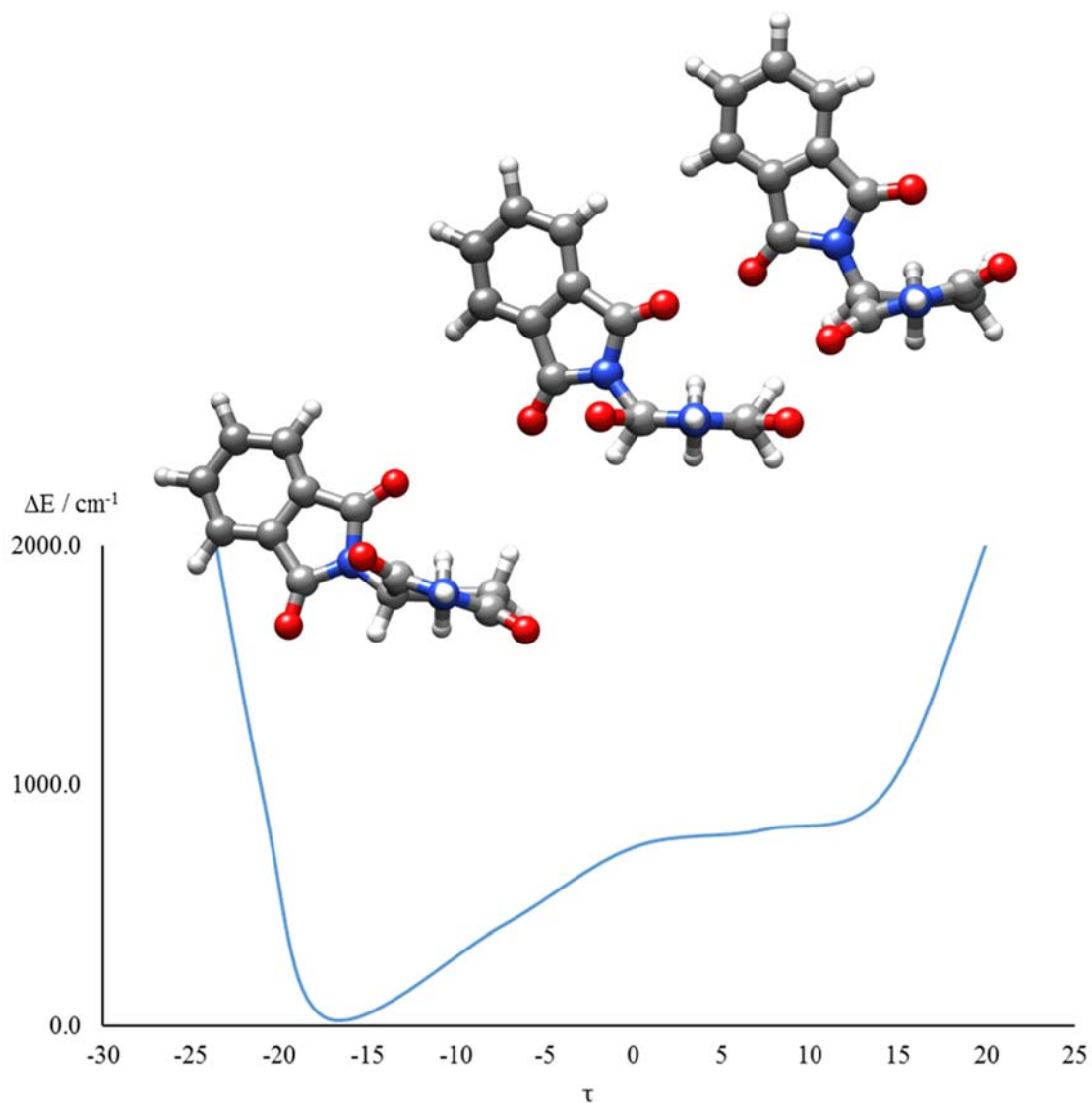


**Figure S8.** DFT Potential energy function (B3LYP-D3BJ/cc-pVDZ) of thalidomide for the pure glutarimide ring twisting coordinate (see Figure S3). The minimum corresponds exactly to the maximum shown in Figure S4 at  $\phi = 0^\circ$  for the ring-bending coordinate.

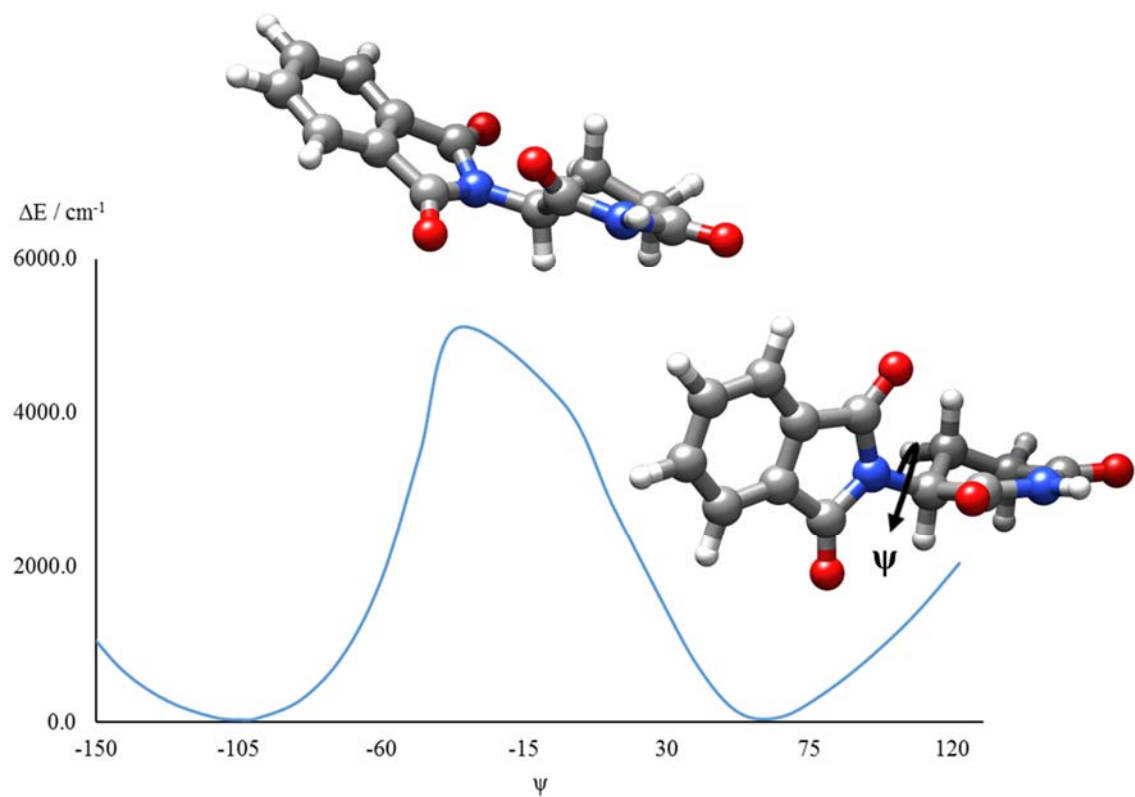


**Figure S9.** DFT Potential energy profile (B3LYP-D3BJ/cc-pVDZ) of thalidomide for internal rotation of phthalimide moiety against glutarimide around the N-C<sub>β</sub> bond for the equatorial form of thalidomide. This periodical motion has a rather high hindering barrier with a very distorted structure.

**Table S1.** Relative intensities for the *o*-anisic acid monomer conformations with respect to the most intense species observed (T1) of the most intense spectra (Ar LA). Eight different spectra were collected taking into account the carrier gas employed, Argon (Ar) or Neon (Ne), the form of volatilizing the sample, heating (Ht) or laser ablation (LA), and the presence (W) or not of a water reservoir in the carrier gas line before the nozzle. All the spectra were taken with the same number of averages (800 kAv), obtaining a similar S/N ratio.

	Ar	Ar	Ar-W	Ar-W	Ne	Ne	Ne-W	Ne-W
	(Ht)	(LA)	(Ht)	(LA)	(Ht)	(LA)	(Ht)	(LA)
<b>T1</b>	32.5	100.0	11.8	65.2	51.4	51.2	25.8	26.7
<b>C1</b>	0.8	2.9	0.2	1.6	1.0	1.4	0.2	0.7
<b>C2(0<sup>+</sup>)</b>	2.3	7.2	0.6	4.3	2.9	4.4	1.4	2.1
<b>C2(0<sup>-</sup>)</b>	-	0.3 <sup>a</sup>	-	0.3 <sup>a</sup>	0.2 <sup>a</sup>	0.4 <sup>a</sup>	0.3 <sup>a</sup>	0.3 <sup>a</sup>
<b>T1-w-1</b>	18.0	2.9	41.5	8.1	97.5	7.5	100.0	9.8
<b>C2-w-1</b>	1.1	0.3 <sup>a</sup>			2.5	0.7 <sup>a</sup>	2.5	

<sup>a</sup> species observed near the limit of detection.

**Table S2.** Comparison of the intensities for the *o*-anisic acid monomer and water complex conformations, salicylic acid (Sal A.), methyl salicylate (Sal M.), and Methyl 2-methoxybenzoate (M2M) observed species relative to the most intense species (T1) of each spectrum. The ratios for different molecular species were taken by comparing the most intense lines of each species. Eight different spectra were collected taking into account the carrier gas employed, Argon (Ar) or Neon (Ne), the form of volatilizing the sample, heating (Ht) or laser ablation (LA), and the presence (W) or not of a water reservoir in the carrier gas line before the nozzle. The other species observed upon heating are. All the spectra were taken with the same number of averages (800kAv), obtaining a similar S/N ratio.

	Ar (Ht)	Ar (LA)	Ar W (Ht)	Ar W (LA)	Ne (Ht)	Ne (LA)	Ne W (Ht)	Ne W (LA)
<b>T1</b>	100.0	100.0	100.0	100.0	100.0	100.0	100.0	100.0
<b>C1</b>	2.3	2.9	1.9	2.5	1.9	2.8	1.0	2.7
<b>C2(0<sup>+</sup>)</b>	7.1	7.2	4.7	6.6	5.7	8.6	5.6	8.0
<b>C2(0<sup>-</sup>)</b>	-	0.3	-	0.4 <sup>a</sup>	0.5 <sup>a</sup>	0.7	1.2 <sup>a</sup>	1.1
<b>T1-w-1</b>	12.9	2.1	29.7	5.8	69.8	5.4	71.6	7.0
<b>C2-w-1</b>	0.8 <sup>a</sup>	0.2 <sup>a</sup>	-	-	1.8	0.5 <sup>a</sup>	1.8	-
<b>Sal A.</b>	1.2	-	3.4	-	1.7	-	3.1	-
<b>M. Sal</b>	1.5	-	4.8	-	1.2	-	5.6	-
<b>M2M</b>	0.8 <sup>a</sup>	-	-	-	0.5 <sup>a</sup>	-	1.0 <sup>a</sup>	-

<sup>a</sup> species observed in the limit of the detection.

**Table S3.** Predicted coordinates of the molecular structure of TD-eq conformer calculated at B3LYP-D3BJ/cc-pVDZ level of theory.

Center Number	Atomic Number	Coordinates (Angstroms)		
		X	Y	Z
1	6	-3.264597	-1.639434	0.175010
2	6	-2.224342	-0.720250	0.189864
3	6	-2.456340	0.649688	0.029941
4	6	-3.737468	1.153136	-0.151380
5	6	-4.795596	0.232667	-0.167620
6	6	-4.562932	-1.141172	-0.007208
7	6	-1.144166	1.356293	0.080989
8	7	-0.186952	0.353116	0.328207
9	6	-0.756880	-0.933325	0.351509
10	8	-0.138528	-1.967945	0.486567
11	6	1.233864	0.602332	0.260448
12	6	2.005151	0.142160	1.499699
13	6	3.490070	0.450671	1.315114
14	6	4.063096	-0.137893	0.040289
15	7	3.153928	-0.286895	-1.012570
16	6	1.793131	-0.010607	-1.031099
17	8	5.225595	-0.451094	-0.104943
18	8	1.114658	-0.217801	-2.013545
19	8	-0.895300	2.535507	-0.048566
20	1	3.535887	-0.678437	-1.872444
21	1	3.650042	1.543343	1.261491
22	1	4.103219	0.079043	2.146440
23	1	1.610673	0.659204	2.386278
24	1	1.847883	-0.937197	1.640001
25	1	1.328235	1.696764	0.150262
26	1	-3.068593	-2.705410	0.297364
27	1	-5.407798	-1.832272	-0.027351
28	1	-5.817735	0.588688	-0.310002
29	1	-3.903672	2.223608	-0.278471

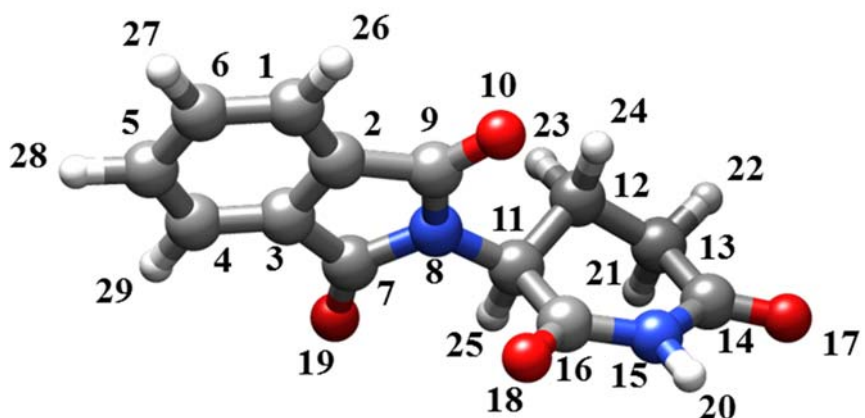


**Table S4.** Predicted coordinates of the molecular structure of TD-eq conformer calculated at MP2/6-311++G(2d,p) level of theory.

Center Number	Atomic Number	Coordinates (Angstroms)		
		X	Y	Z
1	6	-3.224031	-1.642398	0.289668
2	6	-2.201863	-0.707941	0.223233
3	6	-2.459079	0.643115	-0.008564
4	6	-3.749453	1.118813	-0.185112
5	6	-4.789512	0.184148	-0.121413
6	6	-4.531070	-1.174086	0.111904
7	6	-1.160866	1.371178	-0.026573
8	7	-0.185247	0.400508	0.251620
9	6	-0.731629	-0.886818	0.362399
10	8	-0.085867	-1.901265	0.540042
11	6	1.228477	0.651830	0.163827
12	6	1.979072	0.356667	1.456712
13	6	3.461738	0.641306	1.246149
14	6	4.039939	-0.137831	0.089628
15	7	3.146952	-0.422680	-0.946250
16	6	1.794677	-0.124807	-1.024306
17	8	5.200933	-0.491963	0.015178
18	8	1.125947	-0.437776	-1.989131
19	8	-0.935906	2.548088	-0.226855
20	1	3.532791	-0.932964	-1.737041
21	1	3.615725	1.704704	1.026374
22	1	4.059768	0.401755	2.125756
23	1	1.577803	0.983906	2.255933
24	1	1.824479	-0.688890	1.734116
25	1	1.326681	1.717685	-0.082655
26	1	-3.011364	-2.691757	0.467722
27	1	-5.361126	-1.872231	0.152971
28	1	-5.814965	0.513060	-0.256746
29	1	-3.937176	2.172091	-0.367905

**Table S5.** Predicted coordinates of the molecular structure of TD-ax conformer calculated at B3LYP-D3BJ/cc-pVDZ level of theory.

Center Number	Atomic Number	Coordinates (Angstroms)		
		X	Y	Z
1	6	-2.801007	1.897167	0.122346
2	6	-1.946365	0.809860	0.001028
3	6	-2.434381	-0.493386	-0.136981
4	6	-3.796542	-0.760415	-0.158997
5	6	-4.669004	0.331366	-0.038228
6	6	-4.179470	1.638367	0.100352
7	6	-1.270560	-1.420849	-0.230388
8	7	-0.125301	-0.596082	-0.177830
9	6	-0.456641	0.757104	-0.006972
10	8	0.343217	1.664642	0.105569
11	6	1.220587	-1.151946	-0.118410
12	6	2.027017	-1.003513	-1.414194
13	6	2.708499	0.359896	-1.529077
14	6	3.550661	0.678757	-0.314080
15	7	3.106054	0.111025	0.887510
16	6	1.939422	-0.598484	1.122632
17	8	4.539613	1.380453	-0.325628
18	8	1.533827	-0.810967	2.245854
19	8	-1.250436	-2.627641	-0.331037
20	1	3.606129	0.416345	1.721397
21	1	3.363680	0.423010	-2.408011
22	1	1.960921	1.165402	-1.605420
23	1	2.794142	-1.795689	-1.424010
24	1	1.365530	-1.189663	-2.272444
25	1	1.056428	-2.219490	0.086757
26	1	-2.406300	2.907945	0.232617
27	1	-4.884856	2.466172	0.194448
28	1	-5.747548	0.163106	-0.049866
29	1	-4.163768	-1.782065	-0.263775

**Table S6.** Predicted coordinates of the molecular structure of TD-ax conformer calculated at MP2/6-311++G(2d,p) level of theory.

Center Number	Atomic Number	Coordinates (Angstroms)		
		X	Y	Z
1	6	-2.760586	1.890184	0.069901
2	6	-1.913390	0.793575	0.020164
3	6	-2.402136	-0.503547	-0.129568
4	6	-3.760227	-0.762241	-0.234364
5	6	-4.625809	0.336843	-0.183639
6	6	-4.134187	1.641285	-0.033562
7	6	-1.245076	-1.438834	-0.141473
8	7	-0.101610	-0.627147	-0.021904
9	6	-0.429564	0.729782	0.098975
10	8	0.374482	1.633694	0.229149
11	6	1.229509	-1.193035	0.109122
12	6	1.983308	-1.264565	-1.213289
13	6	2.531432	0.102110	-1.604727
14	6	3.420649	0.667814	-0.526467
15	7	3.119643	0.252578	0.775934
16	6	1.992569	-0.432742	1.195124
17	8	4.346636	1.429641	-0.727400
18	8	1.662993	-0.481669	2.364817
19	8	-1.228121	-2.649618	-0.232621
20	1	3.643388	0.720633	1.511672
21	1	3.119217	0.064993	-2.522717
22	1	1.718536	0.818333	-1.759345
23	1	2.810290	-1.972942	-1.098363
24	1	1.318385	-1.662779	-1.983195
25	1	1.075161	-2.200924	0.505934
26	1	-2.368051	2.895193	0.188236
27	1	-4.833495	2.470508	0.003489
28	1	-5.696980	0.179522	-0.260092
29	1	-4.129542	-1.776464	-0.348435















17	4	13	16	17	17	3	15	16	17	5940.	6109	0.0086
17	4	13	18	17	17	3	15	18	17	5940.	6109	0.0086
17	4	13	16	15	17	3	15	16	15	5940.	6109	0.0086
16	4	12	16	16	16	3	14	16	16	5941.	7207	0.0033
16	4	12	17	17	16	3	14	17	17	5941.	7207	0.0033
16	4	12	15	15	16	3	14	15	15	5941.	7207	0.0033
16	4	12	15	17	16	3	14	16	17	5941.	7207	0.0033
16	4	12	12	15	16	3	14	16	15	5941.	7207	0.0033
16	4	12	17	18	16	3	14	17	18	5941.	7207	0.0033
16	4	12	15	16	16	3	14	15	16	5941.	7207	0.0033
16	4	12	17	16	16	3	14	17	16	5941.	7207	0.0033
16	4	12	15	14	16	3	14	15	14	5941.	7207	0.0033
12	4	9	13	14	12	3	9	13	14	5942.	7069	-0.0046
12	4	9	11	12	12	3	9	11	12	5942.	7069	-0.0046
12	4	9	13	12	12	3	9	13	12	5942.	7069	-0.0046
12	4	9	11	10	12	3	9	11	10	5942.	7069	-0.0046
15	4	11	16	16	15	3	13	16	16	5943.	2060	0.0020
15	4	11	14	14	15	3	13	14	14	5943.	2060	0.0020
15	4	11	15	16	15	3	13	15	16	5943.	2060	0.0020
15	4	11	15	14	15	3	13	15	14	5943.	2060	0.0020
15	4	11	14	17	15	3	13	16	17	5943.	2709	0.0087
15	4	11	14	15	15	3	13	14	15	5943.	2709	0.0087
15	4	11	16	15	15	3	13	16	15	5943.	2709	0.0087
15	4	11	14	13	15	3	13	14	13	5943.	2709	0.0087
14	4	10	14	14	14	3	12	14	14	5944.	8313	0.0061
14	4	10	15	15	14	3	12	15	15	5944.	8926	0.0011
14	4	10	13	13	14	3	12	13	13	5944.	8926	0.0011
14	4	10	14	15	14	3	12	14	15	5944.	8926	0.0011
14	4	10	14	13	14	3	12	14	13	5944.	8926	0.0011
14	4	10	15	16	14	3	12	15	16	5944.	9566	-0.0011
14	4	10	13	14	14	3	12	13	14	5944.	9566	-0.0011
14	4	10	15	14	14	3	12	15	14	5944.	9566	-0.0011
14	4	10	13	12	14	3	12	13	12	5944.	9566	-0.0011
21	4	17	20	20	21	3	19	20	20	5945.	8486	0.0031
21	4	17	21	20	21	3	19	21	20	5945.	8991	-0.0052
21	4	17	20	19	21	3	19	20	19	5945.	8991	-0.0052
11	4	8	11	12	11	3	8	11	12	5946.	3517	0.0020
11	4	8	12	12	11	3	8	12	12	5946.	3517	0.0020
11	4	8	11	10	11	3	8	11	10	5946.	3517	0.0020
11	4	8	10	10	11	3	8	10	10	5946.	3517	0.0020
11	4	8	12	13	11	3	8	12	13	5946.	4500	-0.0038
11	4	8	12	11	11	3	8	12	11	5946.	4500	-0.0038
11	4	8	10	11	11	3	8	10	11	5946.	4500	-0.0038
11	4	8	10	9	11	3	8	10	9	5946.	4500	-0.0038
13	4	9	14	14	13	3	11	14	14	5946.	6050	-0.0012
13	4	9	12	12	13	3	11	12	12	5946.	6050	-0.0012
13	4	9	13	14	13	3	11	13	14	5946.	6050	-0.0012
13	4	9	13	12	13	3	11	13	12	5946.	6050	-0.0012
13	4	9	14	15	13	3	11	14	15	5946.	6822	-0.0017
13	4	9	12	13	13	3	11	12	13	5946.	6822	-0.0017
13	4	9	14	13	13	3	11	14	13	5946.	6822	-0.0017
13	4	9	12	11	13	3	11	12	11	5946.	6822	-0.0017
12	4	8	12	12	12	3	10	12	12	5948.	1628	0.0125
12	4	8	13	13	12	3	10	13	13	5948.	2381	-0.0026
12	4	8	11	11	12	3	10	11	11	5948.	2381	-0.0026
12	4	8	12	13	12	3	10	12	13	5948.	2381	-0.0026
12	4	8	12	11	12	3	10	12	11	5948.	2381	-0.0026
12	4	8	13	14	12	3	10	13	14	5948.	3287	-0.0029
12	4	8	11	12	12	3	10	11	12	5948.	3287	-0.0029
12	4	8	13	12	12	3	10	13	12	5948.	3287	-0.0029
12	4	8	11	10	12	3	10	11	10	5948.	3287	-0.0029
10	4	7	10	10	10	3	7	10	10	5948.	9399	0.0006
10	4	7	11	11	10	3	7	11	11	5949.	0610	-0.0050
10	4	7	9	9	10	3	7	9	9	5949.	0610	-0.0050
10	4	7	10	11	10	3	7	10	11	5949.	0610	-0.0050
10	4	7	10	9	10	3	7	10	9	5949.	0610	-0.0050
10	4	7	11	12	10	3	7	11	12	5949.	2006	0.0068
10	4	7	9	10	10	3	7	9	10	5949.	2006	0.0068
10	4	7	11	10	10	3	7	11	10	5949.	2006	0.0068
10	4	7	9	8	10	3	7	9	8	5949.	2006	0.0068
11	4	7	11	11	11	3	9	11	11	5949.	6084	-0.0002
11	4	7	12	13	11	3	9	12	13	5949.	8154	-0.0092
11	4	7	12	11	11	3	9	10	11	5949.	8154	-0.0092
11	4	7	12	11	11	3	9	12	11	5949.	8154	-0.0092
11	4	7	10	9	11	3	9	10	9	5949.	8154	-0.0092
9	4	6	9	9	9	3	6	9	9	5950.	8546	0.0034
10	4	6	10	10	10	3	8	10	10	5950.	8546	0.0034
10	4	6	11	11	10	3	8	11	11	5950.	9781	-0.0115
9	4	6	10	10	9	3	6	10	10	5950.	9781	-0.0115
10	4	6	9	9	10	3	8	9	9	5950.	9781	-0.0115
9	4	6	8	8	9	3	6	8	8	5950.	9781	-0.0115
10	4	6	10	11	10	3	8	10	11	5950.	9781	-0.0115
9	4	6	9	10	9	3	6	9	10	5950.	9781	-0.0115
10	4	6	10	9	10	3	8	10	9	5950.	9781	-0.0115
10	4	6	11	10	10	3	8	9	10	5951.	1233	-0.0014
10	4	6	11	12	10	3	8	11	12	5951.	1233	-0.0014
10	4	6	9	10	10	3	8	9	10	5951.	1233	-0.0014
10	4	6	11	10	10	3	8	11	10	5951.	1233	-0.0014
10	4	6	9	8	10	3	8	9	8	5951.	1233	-0.0014
9	4	6	10	11	9	3	6	10	11	5951.	1233	-0.0014
9	4	6	8	9	9	3	6	8	9	5951.	1602	-0.0058
9	4	6	10	9	9	3	6	10	9	5951.	1602	-0.0058
9	4	6	8	7	9	3	6	8	7	5951.	1602	-0.0058